Machine learning-based identification of pyroptosis-related genes as biomarkers and targets in primary Sjögren's disease

X. Jiang[1], X. Liang[1], Y. Hong[2], C. Hua[3], S. Gao[4], T. Zhang[5]

[1]School of Ophthalmology and Optometry, School of Biomedical Engineering, Wenzhou Medical University, Zhejiang Province; [2]The Second School of Medicine, Wenzhou Medical University, Zhejiang Province; [3]School of Basic Medical Sciences, Wenzhou Medical University, Zhejiang Province; [4]Laboratory Animal Centre, Wenzhou Medical University, Zhejiang Province; [5]Department of Rheumatology, The First Affiliated Hospital of Wenzhou Medical University, Zhejiang Province, China.

Abstract

Objective

Primary Sjögren's disease (pSD) is a chronic autoimmune disease with significant heterogeneity. Pyroptosis, a highly inflammatory programmed cell death, plays a key role in autoimmune diseases, including pSD. However, the role and mechanisms of pyroptosis-related genes (PRGs) in pSD remain unclear.

Methods

This study integrated bioinformatics approaches to analyse gene expression datasets from Gene Expression Omnibus. Differentially expressed genes were identified, followed by weighted gene co-expression network analysis and functional enrichment analysis. Multi-model machine learning frameworks and SHapley Additive exPlanations were used to screen candidate genes. The CIBERSORT algorithm explored the correlation between hub pyroptosis-related and pSD-related genes (PSGs) and immune cell populations, validated by single-cell RNA sequencing data. Nomogram models were developed to assess pSD prevalence, and molecular docking studies predicted potential therapeutic agents targeting these genes.

Results

A total of 647 differentially expressed genes were identified between pSD patients and healthy controls. Through WGCNA and functional enrichment analysis, significant pathways related to oxidative phosphorylation, apoptosis, and cell adhesion were revealed. Machine learning models identified HADHA, JAK1, BRD4, ATG5, and NRAS as hub PSGs with high diagnostic potential. Nomogram models based on these genes showed promising diagnostic accuracy. Molecular docking results suggested that some compounds could modulate the activity of these key genes.

Conclusion

This study provides novel insights into the molecular mechanisms of pSD and highlights potential diagnostic biomarkers and therapeutic targets related to pyroptosis. The integration of bioinformatics and machine learning offers a robust framework for understanding the complex interplay between pyroptosis and pSD pathogenesis.

Key words

primary Sjögren's disease, pyroptosis, biomarker, machine learning, therapeutic target, molecular docking

Xiaoyang Jiang, MD
Xinyue Liang, MD
Yanggang Hong, MD
Chunyan Hua, PhD
Sheng Gao, PhD
Ting Zhang, PhD

Please address correspondence to:
Chunyan Hua
School of Basic Medical Sciences, Wenzhou Medical University, Wenzhou 325035, Zhejiang Province, China.
E-mail: huachunyan@wmu.edu.cn

and to:
Sheng Gao
Laboratory Animal Centre, Wenzhou Medical University, Wenzhou 325035, Zhejiang, China.
E-mail: gaosheng@wmu.edu.cn

Ting Zhang
Department of Rheumatology, The First Affiliated Hospital of Wenzhou Medical University, Wenzhou 325035, Zhejiang, China.
E-mail: asurfer@163.com

Received on August 23, 2025; accepted in revised form on November 13, 2025.

Availability of data and materials
The data supporting the conclusions of this article are available in the article, Supplementary material, and the GEO repository (https://www.ncbi nlm.nih.gov/geo/), Cellmarker2.0 (http://117.50.127.228/CellMarker/), Uniprot database (https://www.uniprot.org/), and PubChem database (https://pubchem.ncbi.nlm.nih.gov/). Further inquiries can be directed to the corresponding authors.

Appendix A. Supplementary data to this article can be found in the online version.

Funding: this study was supported by the Science and Technology Plan Project of Wenzhou Municipality, China (grant nos. Y20220045, Y20220389), and Natural Science Foundation of Zhejiang Province (grant no. LTGY23H100001).

Competing interests: none declared.

Introduction

Primary Sjögren disease (pSD) is a chronic autoimmune disease distinguished by the infiltration of exocrine glands with lymphocytes, predominantly affecting the lacrimal and salivary glands (SG) (1, 2). The estimated prevalence of pSD is 0.3/1000-1/1000, with 30–40% of pSD patients experiencing systemic complications involving multiple organs and systems, such as palpable purpura, cryoglobulinaemia-associated glomerulonephritis, and peripheral neuropathy, ultimately leading to higher mortality rates than the general population (3, 4). The heterogeneity and disabling nature of pSD significantly impact patients' quality of life, highlighting the urgent requirement for enhanced diagnostic and therapeutic methodologies (5). Therefore, revealing the pathogenesis of pSD can improve the diagnosis and targeted treatment of pSD.

Cellular pyroptosis is a highly inflammatory form of programmed cell death mediated by the pore forming activity of the Gasdermin family, leading to cell lysis and release of pro-inflammatory cytokines. The key role of pyroptosis in autoimmune diseases, including pSD, has attracted increasing attention (6). Siqi Yu *et al*. have observed that $KRT14^+$ progenitor cells may undergo pyroptosis in submandibular SG, leading to functional impairments of SG (7). The potential role of caspase-1 increase caused by type I IFN has been found in the pathogenesis of pSD. This process further stimulates the secretion of pro-inflammatory cytokines, which promotes the infiltration and activation of immune cells, and induces dysfunction in surrounding salivary gland epithelial cells (SGECs) (8). In addition, in the ductal epithelial cells of pSD patients, excessive damage to cytoplasmic DNA due to DNase1 deficiency activates absent in melanoma 2 (AIM2) inflammasomes, leading to increased pyroptosis (9). However, there are few studies on pyroptosis-related genes (PRGs) in pSD, and the role and mechanisms of pyroptosis in pSD have yet to be further explored.

Understanding the role of PRGs in pSD is crucial for developing novel diagnostic and therapeutic approaches. The aim of this study is to comprehensively investigate the expression profile of PRGs in pSD. A multi-model machine learning framework and SHapley Additive exPlanations (SHAP) were used to screen candidate genes with high diagnostic potential. Single-cell RNA sequencing data from patients with pSD were used to investigate the expression characteristics of pyroptosis-related and pSD-related genes (PSGs) and the potential regulatory mechanism of pSD. Furthermore, nomograms in two datasets were carried out for validation of the results. Finally, we explored the potential of the key gene as a drug target through molecular docking studies, identifying compounds that could modulate its activity and ameliorate disease symptoms. The exploration of the intricate relationship between pyroptosis and pSD provides novel insights into the pathogenesis of the disease and potential therapeutic targets.

Methods

Data source

The study design is depicted in Figure 1. A comprehensive search was performed on the Gene Expression Omnibus (GEO, https://www.ncbi.nlm.nih.gov/geo/) to identify relevant gene expression datasets. The search terms included "primary Sjögren disease", "primary Sjögren syndrome", "pSD", and "pSS". The dataset selection followed these criteria: 1. inclusion of clearly defined pSD patients and healthy controls (HCs); 2. availability of whole blood or peripheral blood mononuclear cell (PBMC) gene expression profiles to maintain tissue consistency. Based on this, the dataset GSE84844, encompassing 30 pSD samples and 30 HCs, was selected for in-depth analysis. For validation, additional datasets were obtained: GSE66795 (131 pSD patients, 29 HCs, whole blood), GSE51092 (190 pSD patients, 32 HCs, whole peripheral blood), and GSE157278 (5 pSD samples, 5 HCs, peripheral blood, single-cell RNA). The details of the datasets are shown in Supplementary Table S1. PRGs were compiled from various bioinformatics resources, including GeneCards (https://www.genecards.org/),

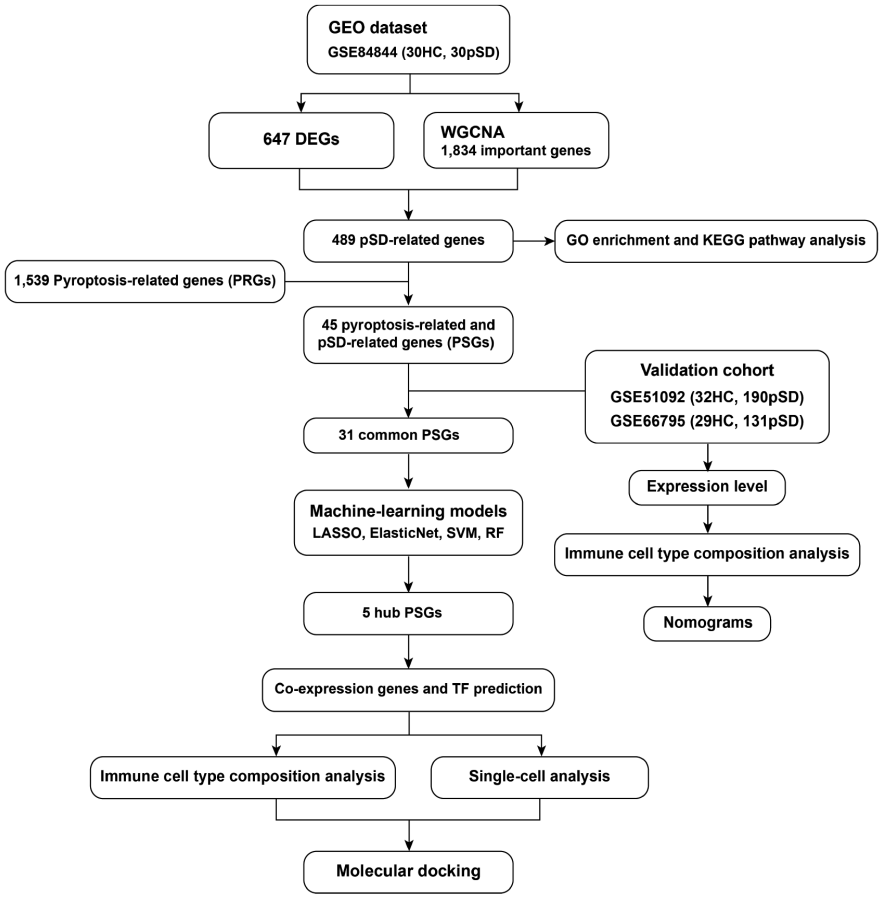

Fig. 1. Workflow diagram of this study.

AmiGO2 (https://amigo.geneontology.org/amigo), MSigDB (https://www.gsea-msigdb.org/gsea/msigdb), Genclip3 (http://cismu.net/genclip3/analysis.php), and relevant literature before February 20, 2024, resulting in a total of 1,539 genes (Suppl. Table S2).

Differentially expressed genes analysis

Differentially expressed genes (DEGs) were identified in GSE84844 using the limma R package (v. 3.58.1) with the threshold |log2 Fold Change| (|log2 FC|) ≥0.5 and adj.P.Val <0.05" The results were visualised using a volcano plot generated by the EnhancedVolcano R package (v. 1.20.0).

Weighted gene co-expression network analysis (WGCNA)

WGCNA, a method commonly used for studying diseases and biological networks, was employed to identify cluster modules and construct a co-expression network matrix for pSD traits using the WGCNA R package (v. 1.72-5) (10). Genes with similar expression profiles were clustered into modules via average linkage hierarchical clustering. The 'pickSoftThreshold' function was applied to determine an optimal soft threshold (range 1–20), facilitating the generation of an adjacency matrix subsequently transformed into a topological overlap matrix. Modules of co-expressed genes were identified through hierarchical clustering, assigning gene dendrograms and module colours based on expression similarity. Pearson correlation analysis was conducted to ascertain the expression profile of each module with clinical parameters, identifying modules significantly associated with pSD for further study. Within the WGCNA workflow, the identification of key genes hinged on an evaluation of gene significance and intramodular connectivity within the previously identified modules significantly associated with pSD. The threshold kWithin >30 was applied to select genes with high intramodular connectivity, reflecting their central role within the module's network. Additionally, the absolute value of gene significance (|GS|) was set to be greater than 0.5, highlighting a stronger association between the genes and the pSD trait or phenotype under investigation. Through this integrated approach, we aimed to pinpoint genes that are not only highly connected within their respective modules but also significantly related to pSD.

Functional enrichment analysis

Functional pathways were elucidated using the ClusterProfiler R package (v. 4.10.1), with a significant threshold of adjusted *p*-value <0.05, for Kyoto Encyclopedia of Genes and Genomes (KEGG) and Gene Ontology (GO) analysis (11-13). Visualisation of quantitative data was enhanced using the R packages GOplot (v. 1.0.2) and ggplot2 (v. 3.5.1).

Predictive model construction usingmultiple machine-learning methods

Predictive models were constructed using ElasticNet, Least Absolute Shrinkage and Selection Operator (LASSO) logistic regression, Support Vector Machine - Recursive Feature Elimination (SVM-RFE), and Random Forest (RF). The selection of these four machine-learning methods was based on their complementary strengths in handling high-dimensional genomic data with a relatively small sample size. LASSO logistic regression, which performs cyclical coordinate descent along a regularisation path, was executed using the glmnet R package (v. 4.1-8) (14). ElasticNet logistic regression, which combines ridge regression and LASSO regression to decrease variance and attempt to improve prediction performance, was applied in the glmnet R package. The RF model, an ensemble learning method that generates multiple independent decision trees, was implemented using the randomForest R package (v. 4.7-1.1) (15). The SVM model, which seeks the optimal separation hyperplane for classifying instances, was analysed using the R packages e1071 (v.

1.7-14) and caret (v. 6.0-94) with five-fold cross-validation (16). The models were established based on the common genes of the training set (GSE84844) and the validation set (GSE66795, GSE51092), and the area under the ROC curve (AUC), sensitivity, specificity, positive predictive value (PPV), and negative predictive value (NPV) of the models in both the training and external validation sets were calculated using the pROC package (v. 1.18.5) and reportROC package (v. 3.6).

Model interpretation and feature importance

Machine learning models are often considered as black boxes because it is difficult to interpret why an algorithm provides accurate predictions for a particular patient cohort. Therefore, we employed SHAP (SHapley Additive exPlanations) to interpret the machine learning model and elucidate the contribution of each feature to the model's predictions. SHAP is a powerful tool that leverages the concept of Shapley values from cooperative game theory to quantify the importance of each feature in the model's decision-making process. For our study, we applied SHAP to our four models to gain insights into the feature importance and interactions of PSGs. The SHAP summary plot provided a visual representation of the feature importance, highlighting which features had the most significant impact on the model's output. Additionally, we examined the SHAP force plots to reveal how changes in feature values affected the model's output. The plots were performed by the shapviz R package (v. 0.9.7).

Identification of hub PSGs

Based on the performance data (AUC, sensitivity, specificity, PPV, and NPV) of the four models, we assigned weights to them (ElasticNet (0.25), LASSO (0.23), SVM (0.26), and RF (0.26)), and then used the mean (|SHAP value|) of the top 8 important genes identified by the models to calculate their weighted importance and the frequency of being selected by the models. Weighted_Score_gene = Σ(mean (|SHAP value|) × Weight_model) / Σ(Weight_model).

Immune cell type composition analysis and correlation with hub PSGs

We utilised the CIBERSORT (v. 0.1.0) package to assess the proportions of immune cells within tissue samples in GSE84844, GSE66795, and GSE51092 (17). This package leverages the CIBERSORT deconvolution algorithm, which integrates input gene expression profiles with the LM22 reference set to infer the immune cell composition of tissues. Box plots were utilised to visualise the distribution of various immune cells between pSD and control groups, while heatmaps illustrated the interrelationships among different immune cell types. Additionally, lollipop charts depicted the correlation between immune cells and hub PSGs.

Single-cell analysis

The scRNA-seq dataset GSE157278 was obtained from the GEO database for single-cell analysis. Data pre-processing and analysis were conducted using the Seurat R package (v. 5.0.3) (18). Cells with fewer than 200 expressed genes or more than 10% mitochondria-related genes were excluded. Following normalisation, the top 3000 highly variable genes from each Seurat object were selected for further analysis using ScaleData, RunPCA, RunTSNE, and RunUMAP. Cell clustering was performed using FindNeighbors and FindClusters functions, and clusters were visualised using uniform manifold approximation and projection (UMAP) plots. Cell types were identified using CellMarker 2.0 (19), and the expression patterns of hub PSGs across different cell types were visualised using the ggSCvis (v. 0.0.2) and ggplot2 R packages.

The activities of hub PSGs were calculated using the AUCell R package (v. 1.24.0). According to the AUC value, gene-expression rankings were built for each cell. The AUC estimates the proportion of genes in the gene set that are highly expressed in each cell. Cells expressing many genes from the gene set will have higher AUC values than cells expressing fewer genes. Then, the cell clustering UMAP embedding was coloured based on the AUC score of each cell to show which cell clusters were active in the PSGs set.

Analysis of hub PSGs and construction of TF-gene regulatory network

The GeneMANIA website (http://genemania.org) (20) was utilised to identify functionally similar genes to the hub genes and to construct a co-expression network. This platform facilitates the prediction of interactions between hub genes and functionally related genes, as well as their physiological and biochemical responses, co-localisation, and protein-protein interaction pathways. Moreover, the NetworkAnalyst platform was used to construct the transcription factor (TF)-gene regulatory network and the TF-miRNA regulatory network. The JASPAR database (https://jaspar.elixir.no/) (21), integrated within the NetworkAnalyst platform, was utilised for the TF-gene regulatory network analysis. The RegNetwork database (http://www.regnetworkweb.org) (22) served as the source for the TF-miRNA regulatory network.

Validation of hub PSGs

In our quest to ascertain the consistency and specificity of hub PSGs across distinct datasets, we conducted an expression level validation of these genes within the GSE51092 pSD expression profile dataset and the GSE66795 pSD expression profile dataset. The results were graphically represented using the ggplot2 package. Immune cell type composition analysis was also applied to verify the correlation between hub PSGs and immune cells.

Nomogram construction

A nomogram was developed using the rms R package (v. 6.8-0) to assess the incidence of pSD across different clusters. Each predictor contributed to a cumulative score, referred to as the 'total score'. The predictive accuracy of the nomogram was appraised using calibration curves and Decision Curve Analysis (DCA).

Molecular docking

To explore drug-protein interactions, we embarked on a series of molecular dock-

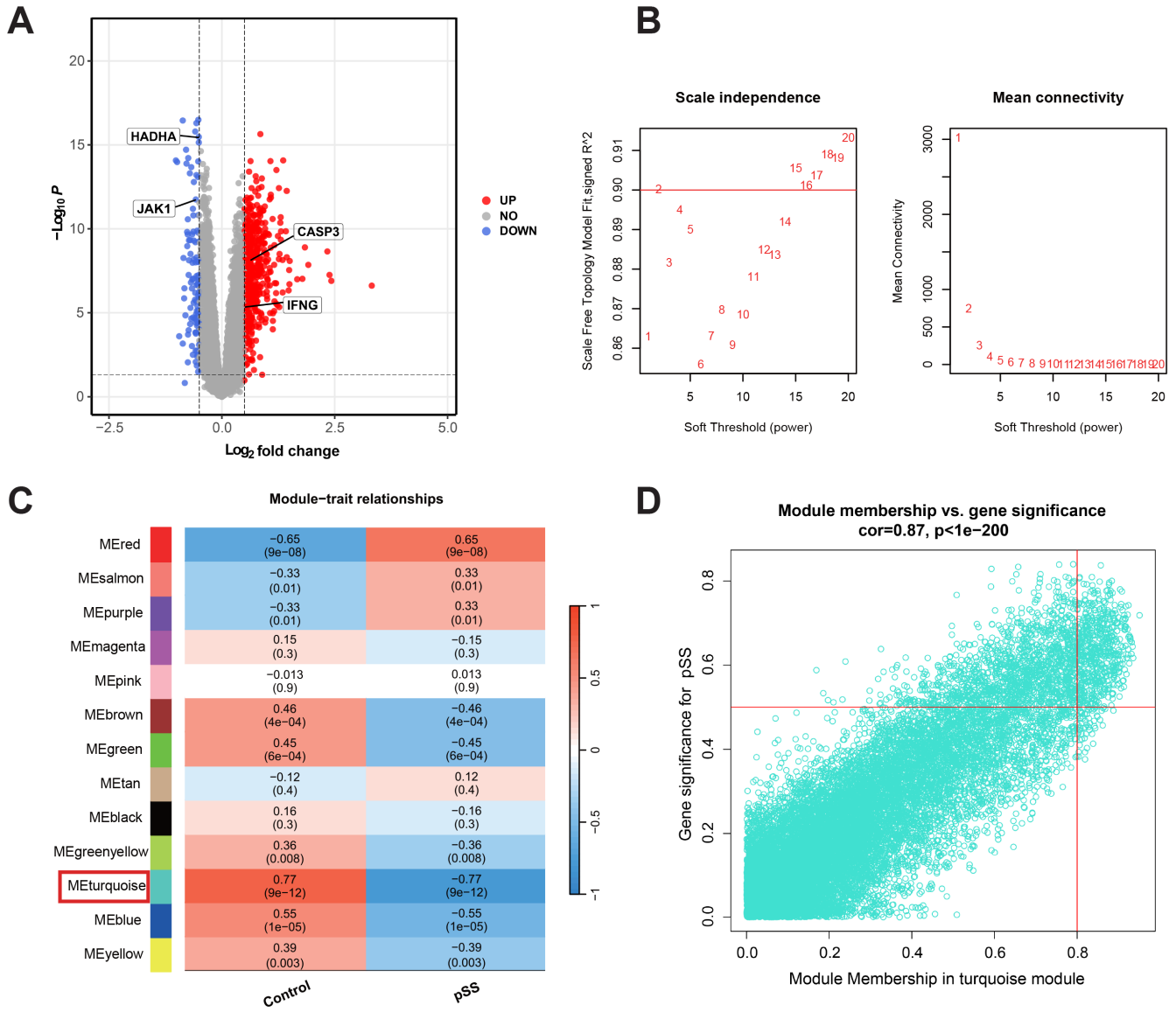

Fig. 2. Differential gene expression analysis and WGCNA of GSE84844 dataset. **A**: The volcano plot visualises the DEGs between pSD and control samples. **B**: Analysis of the scale-free ft index and mean connectivity for various soft-thresholding powers. **C**: Heatmap of module-trait relationships in pSD. Each cell contains the corresponding correlation and *p*-value. **D**: Scatter plot of gene significance *vs*. module membership in the most meaningful module (turquoise module, Cor=0.87, *p*<1e-200).

ing analyses. Enrichr (https://maayanlab.cloud/Enrichr/) is a robust web-server that contains many types of datasets, among which we used the DisgDB database to identify potential drug substances associated with our study (23, 24). Statistical significance was set at <0.05. The molecular structures of the target proteins and ligands were obtained from the UniProt database (https://www.uniprot.org/) and the PubChem database (https://pubchem.ncbi.nlm.nih.gov/). The molecular docking process was executed with AutoDock Vina software (v. 1.5.7) (25) and visualised with PyMol software (v. 2.6.0a0) (26).

Statistical analysis

All statistical analyses were performed using R (v. 4.3.3). Spearman and Pearson correlation were adopted to analyse correlations between PSGs and immune cells. For group comparisons of hub gene expression in validation sets, the Wilcoxon-Mann-Whitney test was employed. In all analyses, a *p*-value <0.05 was considered statistically significant.

Results

Identification and characterisation of pSD-associated gene expression patterns

To elucidate the molecular underpinnings of pSD, we performed a comprehensive analysis of gene expression profiles using the GSE84844 dataset. Differential expression analysis comparing 30 pSD samples with 30 HCs revealed 647 DEGs, comprising 544 upregulated and 103 downregulated genes (Suppl. Table S3). The volcano plot illustrates the distribution of these DEGs, highlighting the substantial transcriptional alterations associated with pSD (Fig. 2A). Subsequently, WGCNA was performed, resulting in the identification of 13 distinct co-expression modules, each represented by a unique colour. A heatmap was generated to illustrate the rela-

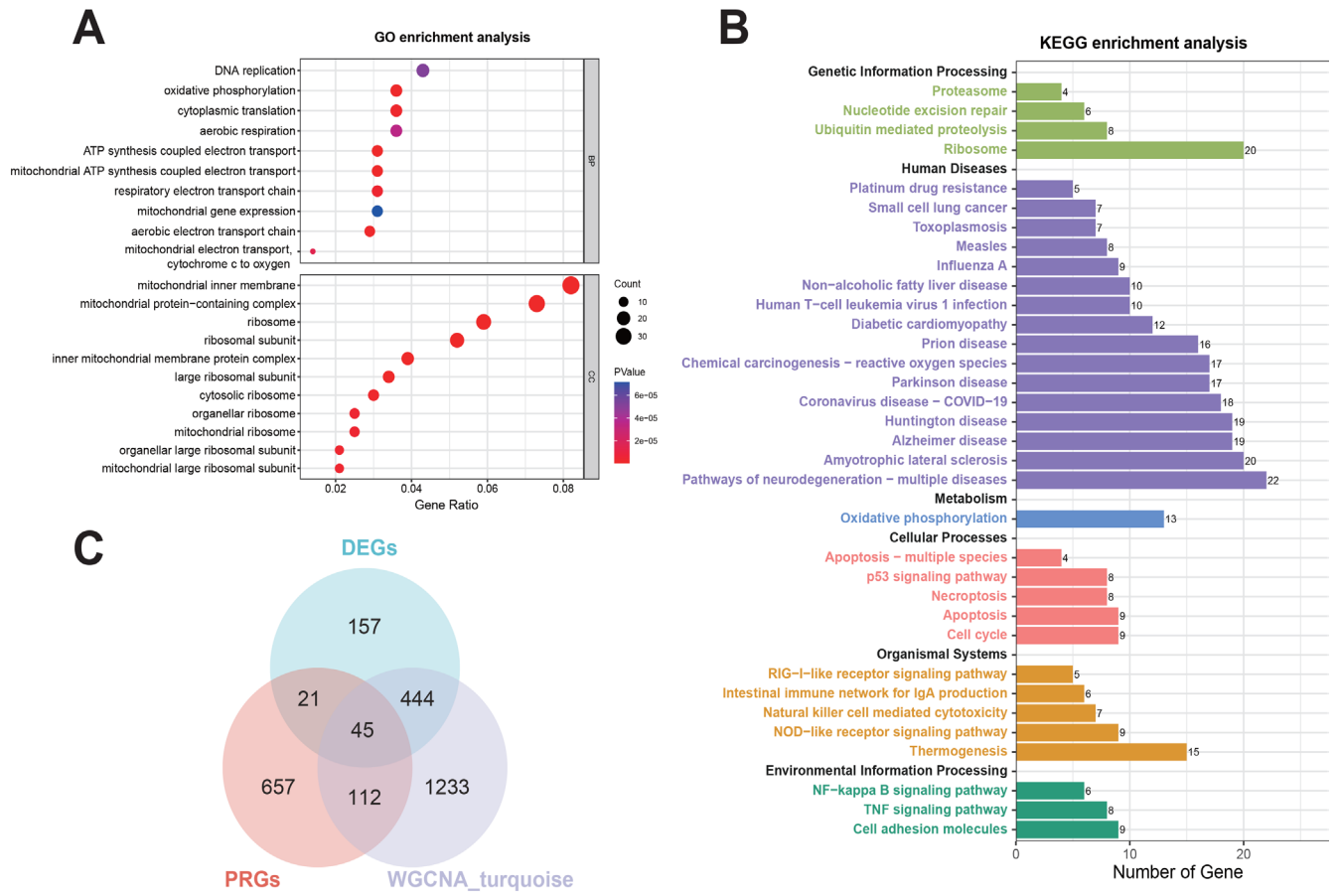

Fig. 3. Functional enrichment analysis of PSGs. **A**: GO enrichment analysis. **B**: KEGG enrichment analysis. Adjusted *p*-value <0.05 was considered significant. **C**: Venn diagram of intersections between PRGs and pSD-related genes.

tionships between these modules and the disease phenotype, based on Spearman correlation coefficients (Fig. 2B, C). Notably, the 'turquoise' module demonstrated the strongest correlation with pSD (Cor=0.87, *p*<1e-200) (Fig. 2D), encompassing a total of 14,385 genes (Suppl. Table S4). We filtered out 1,834 important genes from this module for further analysis. An intersection analysis revealed the pSD-related genes by cross-referencing the genes with the turquoise module with the identified DEGs.

Functional enrichment and pathway analysis of pSD-related genes

Functional enrichment and pathway analyses of 489 pSD-related genes were performed. The GO biological processes (BP) analysis revealed significant alterations in cellular respiration processes, including ATP synthesis coupled electron transport, oxidative phosphorylation, and mitochondrial gene expression. The cell component (CC) analysis highlighted a notable enrichment of mitochondrial components, such as mitochondrial inner membrane, mitochondrial protein-containing complex, and respiratory chain complex (Fig. 3A, Suppl. Table S5). Recent research indicates that mitochondrial dysfunction is closely related to pyroptosis. Mitochondrial-related changes, such as alterations in the permeability of the inner and outer mitochondrial membranes and the release of cytochrome C, can trigger pyroptosis (27). Meanwhile, the activation of inflammatosomes during pyroptosis interacts with mitochondrial dysfunction, which echoes the significant changes in the expression and pathways of mitochondrial-related genes discovered in this study.

Furthermore, KEGG pathway analysis indicated significant enrichment in signalling pathways related to oxidative phosphorylation, apoptosis, cell cycle, and cell adhesion molecules (Fig. 3B, Suppl. Table S6). Pyroptosis has a complex interaction network with other forms of cell death, such as apoptosis and programmed necrosis. Under specific conditions, they can transform into each other or act synergously (28). The enrichment of related pathways, such as apoptosis and cell cycle, further supports the complexity and diversity of cell death-related mechanisms in pSD.

PRGs analyses in pSD-related genes and selection of hub PSGs

To identify PSGs, we intersected PRGs with pSD-related genes, yielding 45 common targets (Fig. 3C), and the expression profiles of these genes were visualised in a heatmap (Suppl. Fig. S1a). Subsequently, we employed multiple machine-learning approaches to refine our gene selection. The dataset GSE84844 was used as the training set, and GSE66795 and GSE51092 as the external validation sets. We built the models based on the 31 common genes of these three datasets. LASSO regression identified 8 genes with the strongest correlation to pSD: HADHA, JAK1, NRAS, BRD4, ATG5, SPRED1, TNFS-

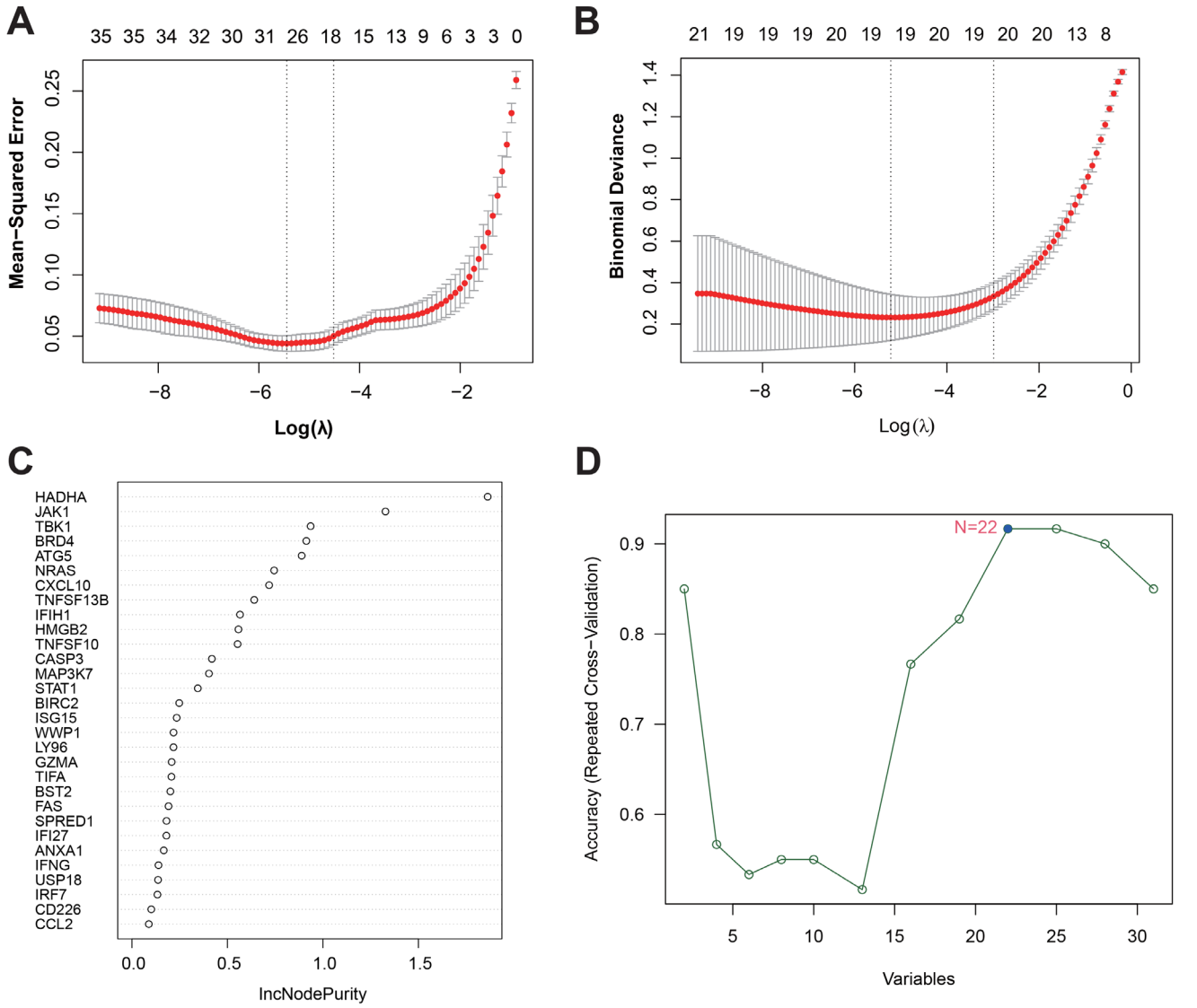

Fig. 4. Identification of hub PSGs through machine learning algorithm. **A**: LASSO model for gene target screening in the 10-fold cross-validation. **B**: The ElasticNet model for gene target screening in the 10-fold cross-validation. **C**: The importance of PSGs based on RF model. A larger IncNodePurity indicates that the variable is more useful in identifying pSD. **D**: The PSGs recognised using SVM-RFE algorithm.

F13B, and WWP1, while ElasticNet identified 15 genes (Fig. 4A, B). Further analysis using RF (Fig. 4C) and SVM models (Fig. 4D) highlighted HADHA and JAK1 as potential hub diagnostic genes (Suppl. Table S7).

The SHAP plots illustrate the importance of each feature in the machine models for predicting pSD, which highlight HADHA as the most dominant feature across all models, consistently contributing the highest to the predictions. Secondary features such as JAK1 and BRD4 also play significant roles but vary slightly in importance depending on the model (Fig. 5A-D). To visually explain how these features affect the model prediction, a force plot shows PSGs in orange contribute to a higher risk of pSD (Fig. 5E).

To further screen the genes, we calculated the AUC, sensitivity, specificity, PPV, and NPV values of each model in the training set and the validation set and comprehensively evaluated the predictive performance of the models (Suppl. Table S8). Among them, the NPV was generally low in the validation cohorts, which suggests that the model may have limitations in excluding negative cases, possibly due to the scarcity of HCs in the validation cohorts. Overall, compared with LASSO model, ElasticNet, RF, and SVM models have better generalisation capabilities. Then, the weighted importance scores were calculated for the genes selected by the model. The final selection of five genes, HADHA, JAK1, BRD4, ATG5, and NRAS, was based on two main criteria: the primary criterion was the frequency of a gene's selection across models, and the secondary criterion was its performance-weighted importance score (Suppl. Table S9).

Functional and regulatory network analysis of hub genes in pSD

The five hub genes (HADHA, JAK1, BRD4, ATG5, and NRAS) were further investigated to elucidate their biological functions and regulatory mechanisms. We constructed a comprehensive gene interaction network utilising

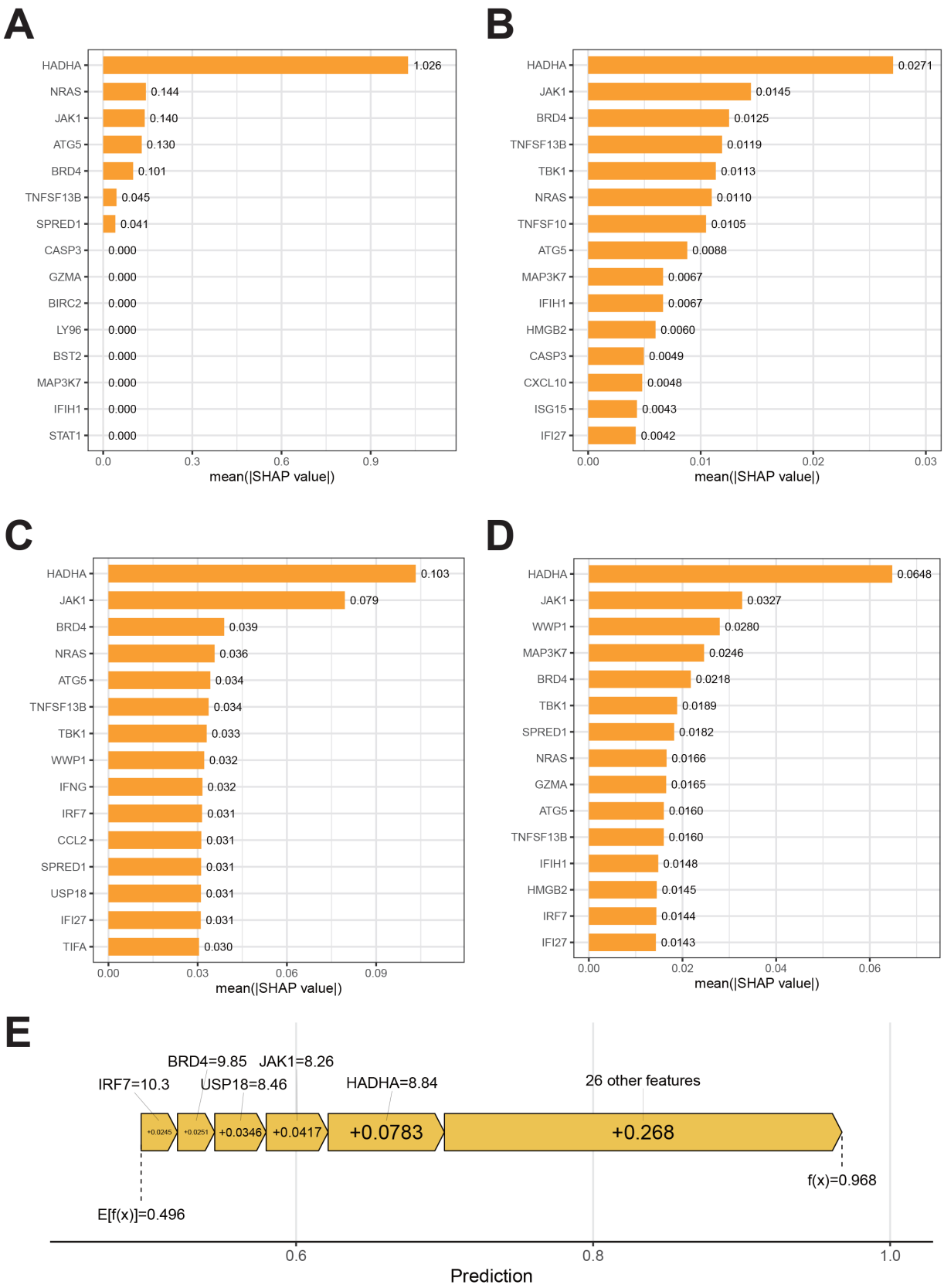

Fig. 5. Identification of hub PSGs through SHAP. **A**: The importance ranking of the top 15 features according to the mean (|SHAP valuel) of LASSO model. **B**: The importance ranking of the top 15 features according to the mean (|SHAP valuel) of ElasticNet model. **C**: The importance ranking of the top 15 features according to the mean (|SHAP valuel) of RF model. **D**: The importance ranking of the top 15 features according to the mean (|SHAP valuel) of SVM model. **E**: Force plot visualised individual model prediction as result of feature contributions.
The higher SHAP value of a feature is given, the higher risk of pSD the patient would have.

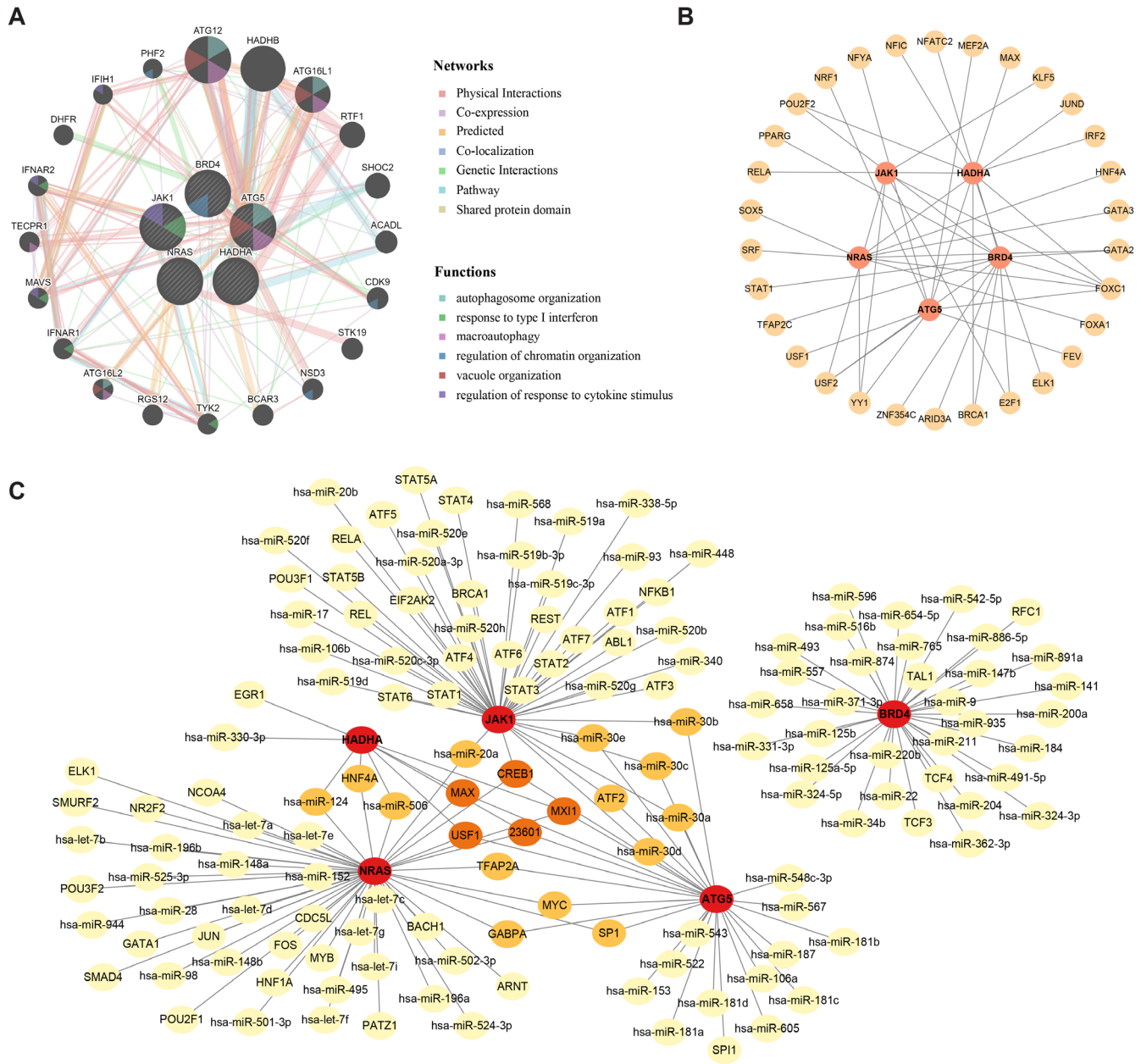

Fig. 6. Co-expression, TF-gene interaction, and TF-miRNA co-regulatory networks of hub PSGs. **A**: Hub PSGs and their co-expression genes were analysed via GeneMANIA. **B**: Network for TF-gene interaction with hub PSGs. The highlighted red colour node represents the hub genes and other nodes represent TF-genes. **C**: Network for TF-miRNA co-regulation.

the GeneMANIA database to elucidate the biological functions of the identified hub genes. The network revealed that physical interactions accounted for 70.90% of the connections, followed by physical interactions (77.64%), co-expression (8.01%), predicted interactions (5.37%), co-localisations (3.63%), genetic interaction (2.87%), pathway (1.88%), and shared protein domains (0.60%) (Fig. 6A). A total of twenty genes associated with the five hub genes were identified, primarily linked to critical biological processes such as autophagosome organisation, macroautophagy, vacuole organisation, regulation of chromatin organisation, and response to type I interferon. The activation of the cGAS/STING pathway is crucial for responding to the secretion of type I interferons and pro-inflammatory cytokines, and is involved in the pyroptosis process (29).

Furthermore, we employed NetworkAnalyst to predict TFs interacting with the hub genes, visualising the TF-gene regulatory network using Cytoscape (Fig. 6B). The network comprised 35 nodes and 42 edges, with several TFs regulating multiple hub genes. FOXC1, POU2F2, and YY1 indicated a higher degree of interaction with the hub genes. Additionally, we constructed a TF-miRNA co-regulatory network, predicting interactions among TFs, miRNAs, and hub genes, which included 150 nodes and 169 edges (Fig. 6C).

Immune cell type composition and hub PSGs correlations in pSD

To explore immune cell type composition in pSD, we applied the CIBER-

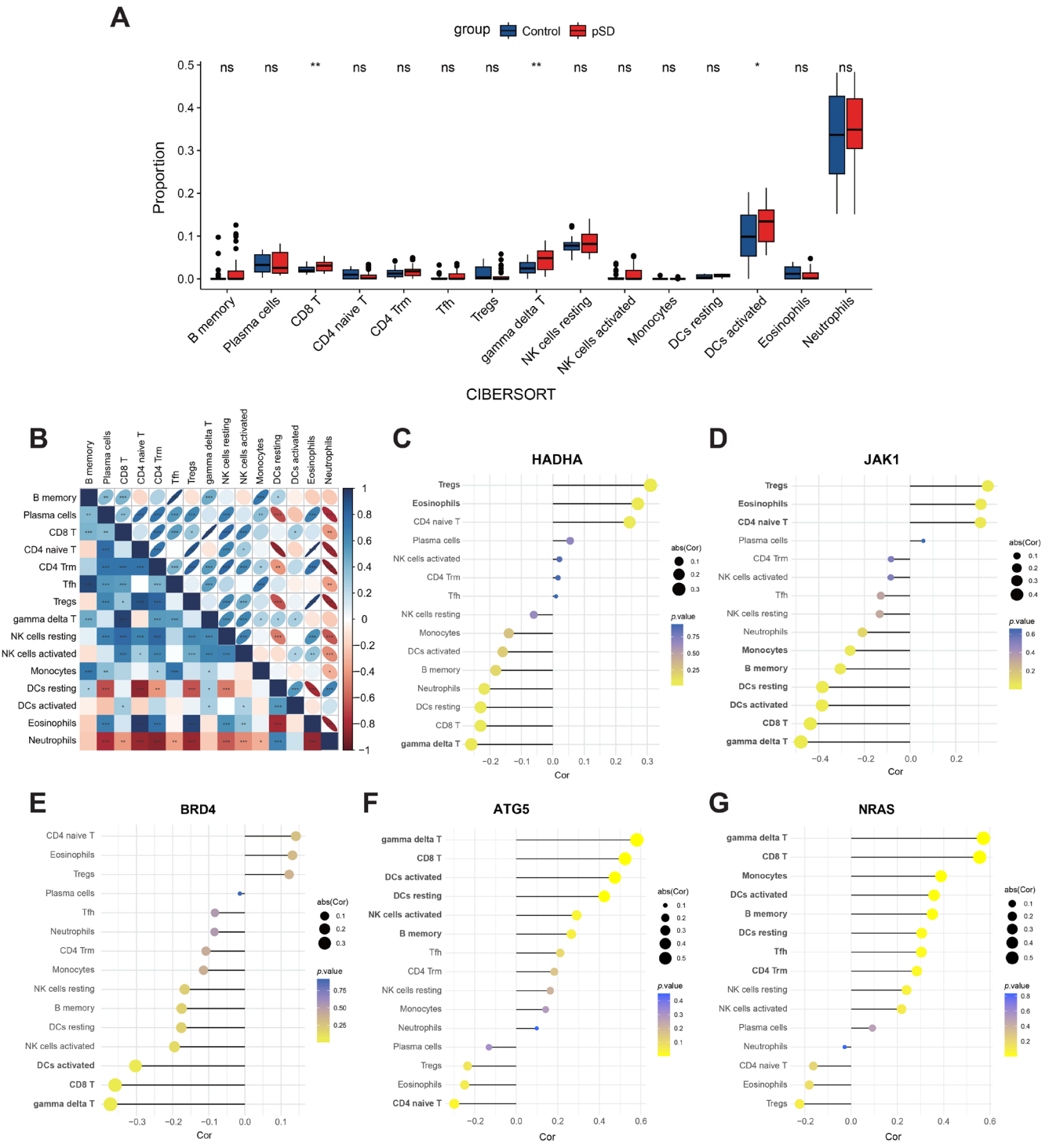

Fig. 7. The correlation between the hub PSGs and immune cells. **A**: The proportion of immune cells in the pSD and control groups. **B**: The correlation of immune cells in pSD tissues was evaluated. Blue: positive correlation; red: negative correlation. **C-G**: The correlation between hub PSGs and immune cells. (*p<0.05, **p<0.01, ***p<0.001).

SORT algorithm to assess immune cell types between pSD patients and controls (Suppl. Fig. S1b). Notably, the proportions of CD8$^+$ T cells, gamma delta T cells, and activated dendritic cells (DCs) were significantly elevated in pSD patients compared to controls (p<0.05) (Fig. 7A). Additionally, correlation analysis between immune cell populations highlighted several key interactions. Gamma delta T cells were positively related to CD8$^+$ T cells and NK cells, while CD8$^+$ T cells were positively related to CD4$^+$ T cells and memory resting (Trm) (Fig. 7B). These interactions suggest a distinct shift in immune cell dynamics associated with pSD pathology.

To further investigate the relationship between hub PSGs expression and immune cell abundance, we performed correlation analysis for selected hub genes, including HADHA, JAK1, BRD4, ATG5, and NRAS, against im-

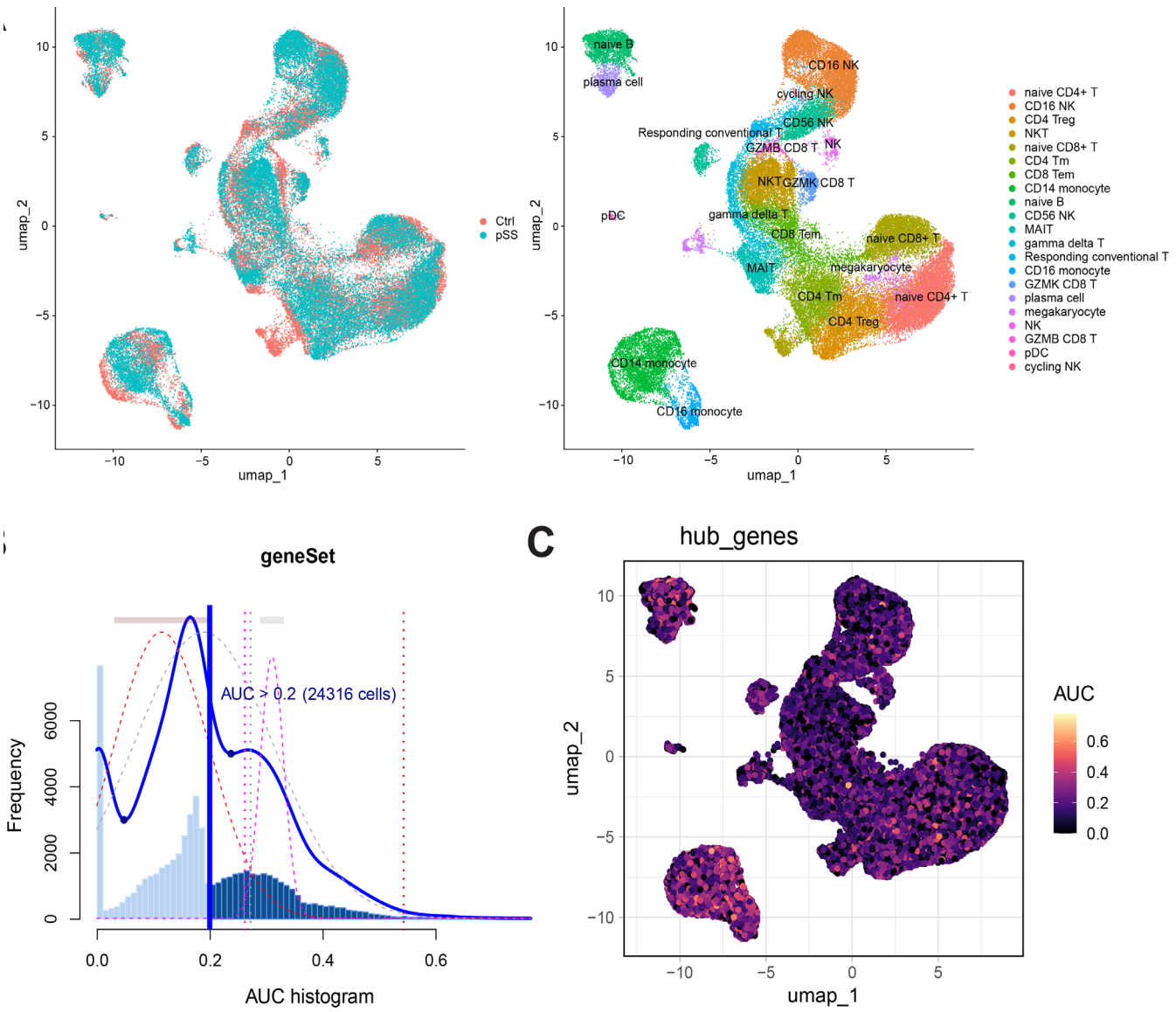

Fig. 8. Expression of hub PSGs at the single-cell level. **A**: UMAP visualisation GSE157278 scRNA-seq datasets. Different colours indicate distinct cell types. **B**: Score of 5 hub PSGs sets. The threshold was chosen as 0.2 and the PSG score of 22036 cells exceeded the threshold value. **C**: UMAP plots based on the PSG score of each cell. High PSG score cell clusters are highlighted.

mune cell populations. HADHA, JAK1, and BRD4 showed positive correlations with T cells regulatory (Tregs), and negative associations with gamma delta T cells and CD8+ T cells. In contrast, ATG5 and NRAS were positively correlated with gamma delta T cells, CD8+ T cells, and DCs (Fig. 7C-G). These findings suggest that these hub PSGs may play crucial roles in modulating immune cell composition and immune responses in pSD.

Single-cell expression profiling of key genes in pSD

We analysed the expression of HADHA, JAK1, BRD4, ATG5, and NRAS at the single-cell level using a subset of 5 pSD patients and 5 normal controls from the GSE157278 dataset. The Seurat pipeline facilitated the identification of various cell populations, including naive CD4 T cells, CD4 Treg, natural killer (NK) cells, CD4 T memory, gamma delta T, naive B cells, and pDCs (Fig. 8A). The distribution of HADHA, JAK1, BRD4, ATG5, and NRAS was visualised, revealing that they were broadly expressed across single-cell subgroups, predominantly in monocytes, NK cells, and CD4+ T cells (Suppl. Fig. S2). Violin plots further indicated that HADHA, JAK1, and ATG5 showed significant differences in expression among various immune cells, such as CD14 monocytes, CD4 Treg, and naive B cells (Suppl. Fig. S2).

In order to further identify the cells involved in hub PSGs, PSG activity for each cell was calculated. Cells expressing many genes from the gene set will exhibit higher AUC values than cells expressing fewer genes. We found two peaks in the AUC values of all cells, while 22036 cells showed relatively higher AUC values when the AUC value threshold was set to 0.2 (Fig. 8B). These cells were mainly in monocytes, naive B cells, plasma cells, naive CD8+ T cells, and naive CD4+ T cells (Fig. 8C). These findings underscore the

Table I. Molecular docking results between potential drugs and hub PSGs (top 10).

PubChem CID	Chemical composition	Target	PDB ID	Binding energy /kcal•mol^{-1}
9552079	CHX	JAK1	3EYG	-9.2
28417	Danazol	HADHA	5ZQZ	-9.1
9552079	CHX	HADHA	5ZQZ	-9.1
28417	Danazol	JAK1	3EYG	-8.9
28417	Danazol	ATG5	4GDK	-8.6
6741	MP	ATG5	4GDK	-8.3
28417	Danazol	NRAS	3CON	-8.1
9552079	CHX	BRD4	2NNU	-8.1
9552079	CHX	NRAS	3CON	-7.7
6741	MP	BRD4	2NNU	-7.7

pivotal role of these hub genes in the monocyte-macrophage system's activity and T cells, aligning with previous immune cell type composition analyses. The comprehensive single-cell expression profiling provides insights into the molecular mechanisms underlying pSD pathogenesis.

Validation of the expression and prediction capacity of hub PSGs

Two external validation datasets (GSE51092, GSE66795) were used to validate the expression levels of hub genes. The results demonstrated that HADHA was significantly downregulated in pSD (Suppl. Fig. S3A-B). As in previous correlation analysis, the heatmaps illustrated that hub PSGs are remarkably related to monocytes, activated DCs, and gamma delta T cells (Suppl. Fig. S3C-D). Interestingly, monocytes occupy a large proportion of the immune microenvironment in validation datasets, and activated DCs were significantly elevated in patients (Suppl. Fig. S4).

To further assess and verify the predictive efficiency of hub PSGs, two nomograms were constructed (Suppl. Fig. S5). In the model, a higher nomogram score indicated a higher probability of disease onset, as shown by the examples of HCs and pSD (Suppl. Fig. S6). In a bid to evaluate the reliability of the nomogram, we established a calibration curve and DCA (Suppl. Fig. S5C-F). According to the calibration curve, the error between the predicted risk and the actual risk was very small (Suppl. Fig. S5C, D). Additionally, the clinical decision curve further confirmed the value of hub genes as diagnostic indicators for pSD (Suppl. Fig. S5G, H).

Molecular docking analysis identifies HADHA as a promising therapeutic target

To explore the potential of 5 hub PSGs as therapeutic targets, we utilised the DisgDB database and selected 8 candidate drugs based on the *p*-value and combined score to conduct molecular docking studies. A binding energy of less than -5 kcal/mol was considered indicative of significant binding activity. As shown in Table I and Supplementary Table S10, chlorhexidine (CHX) had the potentially high binding

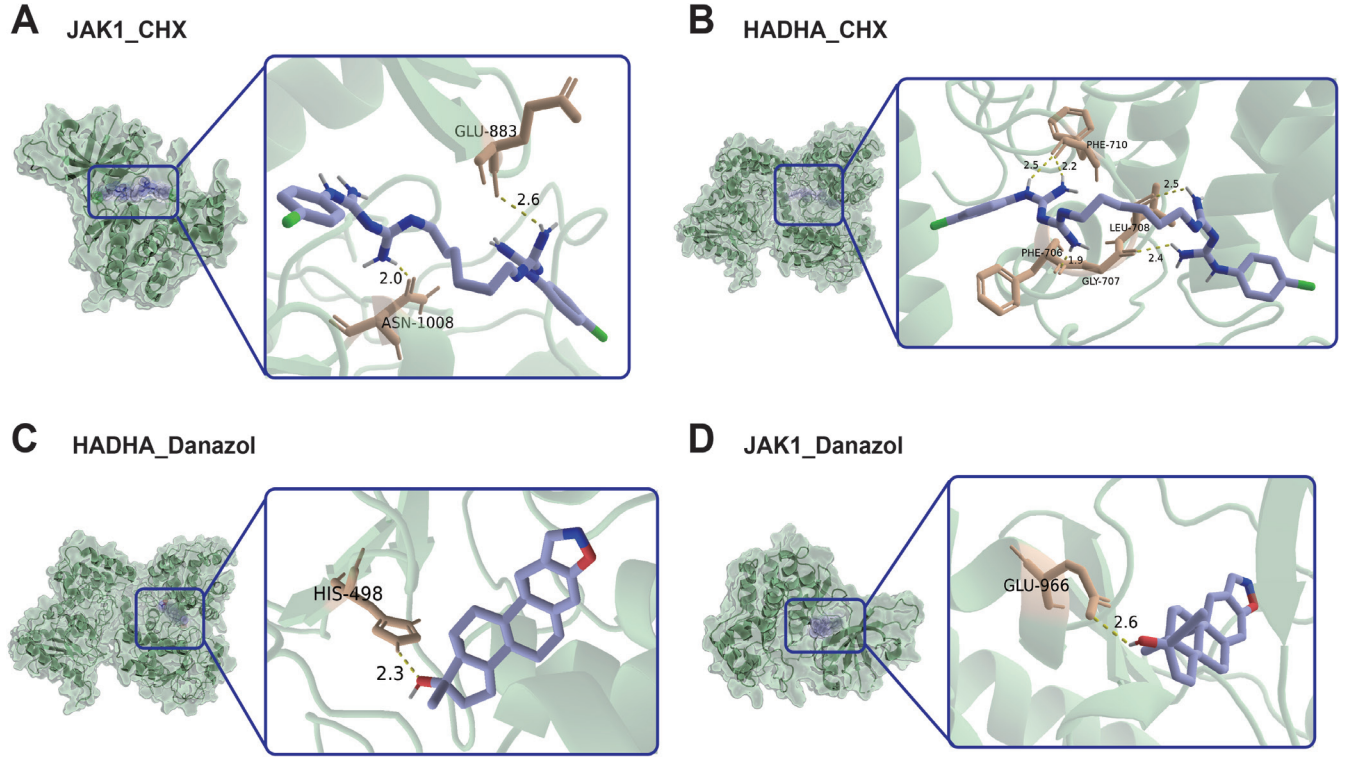

Fig. 9. Prediction of drug targets. **A**: Molecular docking diagram of CHX and JAK1 (PDB: 3EYG). **B**: Molecular docking diagram of CHX and HADHA (PDB: 5ZQZ). **C**: Molecular docking diagram of Danazol and HADHA (PDB: 5ZQZ). **D**: Molecular docking diagram of Danazol and JAK1 (PDB: 3EYG).

affinity with JAK1, HADHA, BRD4, and NRAS, danazol had the potentially high binding affinity with HADHA, JAK1, ATG5, and NRAS, methylprednisolone (MP) had the potentially high binding affinity with ATG5 and BRD4, and so on. Three-dimensional binding modes of the active compounds and proteins were shown in Figure 9. The docking interactions revealed specific binding sites and interactions: CHX interacted with GLU-883 and ASN-1008 of JAK1, forming hydrogen bonds with PHE-706, GLY-707, LEU-708, and PHE-710 of HADHA. Danazol formed hydrogen bonds with HIS-498 of HADHA, and also showed interactions with GLU-966 of JAK1. These findings suggest that these PSGs hold promise as a valuable target for drug therapy in pSD.

Discussion

pSD is a complex autoimmune disorder characterised by immune dysregulation and glandular dysfunction. However, the role and mechanisms of pyroptosis in pSD remain largely unclear (30). Our research delves into a relatively novel aspect of pSD pathogenesis: the interaction between pSD and pyroptosis. By integrating bioinformatics and machine-learning approaches, our research elucidates the molecular underpinnings of pSD and identifies prospective therapeutic targets. The investigation into the nexus between pSD and pyroptosis sheds light on the immune dysregulation of the disease and paves the way for new therapeutic strategies.

In our study, we identified 647 DEGs between pSD patients and healthy volunteers from the GSE84844 dataset and then determined the gene module containing 14385 genes with the highest association with pSD through WGCNA. We obtained 459 pSD-related genes by intersecting DEGs and module genes. Through GO and KEGG pathway enrichment analysis, we found that changes in signalling pathways were mainly enriched in oxidative phosphorylation, cell apoptosis, cell cycle, and cell adhesion molecules. Subsequently, pSD-related genes intersected with 1,539 PRGs, yielding 45 common targets. Employing machine-learning techniques, we identified HADHA, JAK1, BRD4, ATG5, and NRAS as hub PSGs.

HADHA encodes the alpha subunit of mitochondrial trifunctional proteins and plays a critical role in the beta-oxidation of long-chain fatty acids within mitochondria (31). Previous studies have indicated that the deacetylation of HADHA contributes to cardiomyocyte pyroptosis in septic shock (32). In this study, the importance score of HADHA was the highest, and it was consistently downregulated in pSD, which is associated with impaired oxidative phosphorylation and ROS accumulation in immune cells. Mitochondrial ROS activates NLRP3 inflammasome, triggering caspase-1-dependent pyroptosis and IL-1β release, thereby recruiting $CD8^+$ T cells and gamma delta T cells (33-36). A Mendelian randomisation study found that mitochondrial-related proteins are involved in the immune response in autoimmune diseases by influencing cellular energy metabolism (37). This is consistent with studies on mitochondrial dysfunction exacerbating autoimmune inflammation through inflammasome activation. Its robust diagnostic performance and central role in a key pathogenic pathway position HADHA as a compelling candidate for further development as a biomarker.

JAK1, a key mediator of cytokine signalling, showed strong associations with immune cell dynamics, supporting its role in amplifying type I interferon signatures observed in pSD (38). JAK1 is also pivotal in mediating gene expression related to inflammation. In animal models of pSD, inhibition of JAK1 expression has been shown to improve SG function and modulate B cell activity (39). The central role of JAK1 substantiates the therapeutic rationale for exploring JAK inhibitors in pSD, aligning with emerging clinical interests. JAK1 is a central element of the IL-6/JAK1/STAT3 signalling pathway, which is a therapeutic target for mitigating cytokine storms. IL-6, a pro-inflammatory cytokine implicated in B cell proliferation and differentiation (40), is upregulated in the SG and serum of pSD patients (41). Active caspase-1 has been found to directly or indirectly regulate the production of IL-6 (42). Notably, levels of active caspase-1 in the saliva and SG cells of pSD patients are elevated compared to those of healthy individuals (8). Furthermore, the JAK/STAT signalling pathway, a common downstream effector of IFN-γ, is associated with critical biological processes such as cell proliferation, differentiation, apoptosis, and immune modulation (43, 44). Dysregulation of the JAK/STAT pathway has been implicated in the progression of several systemic autoimmune diseases, including rheumatoid arthritis, myeloproliferative neoplasms, and systemic lupus erythematosus (45-47). The prominence of JAK1 supports the investigation of JAK inhibitors (*e.g.* tofacitinib, baricitinib) for pSD treatment, particularly for patients with strong interferon signatures or IL-6 driven inflammation (48). Future clinical trials could stratify patients based on JAK1 expression or related pathway activity to enhance therapeutic precision.

BRD4 is an epigenetic regulatory factor that may drive SGEC pyroptosis by amplifying NF-κB-dependent NLRP3 and IL-1β transcription (49, 50). Conversely, ATG5, a key autophagy protein, appears to play a protective role. Impaired ATG5 function can disrupt mitophagy, exacerbate mitochondrial damage, and facilitate mtDNA release, thereby activating the pro-pyroptotic cGAS-STING-NLRP3 axis in macrophages (51). Therapeutically, strategies to enhance ATG5-mediated autophagy might mitigate pyroptosis and glandular damage in pSD (52). The inclusion of both BRD4 and ATG5 underscores the complex regulatory network governing pyroptosis in pSD.

NRAS is an N-ras oncogene that encodes a membrane protein that shuttles between the Golgi apparatus and the plasma membrane, and has intrinsic GTPase activity. Yang *et al.* believe that NRAS may be involved in the pyroptosis process in ovarian cancer, but the specific mechanism still requires further verification (53). Given its potential role in immune cell signalling and pyroptosis, NRAS warrants further investigation as a modifier of immune cell function in pSD, and its downstream pathways, such as MAPK/ERK

pathway, may represent additional therapeutic avenues (54).

Our immune cell type composition analysis revealed significant shifts in immune cell populations, including elevated $CD8^+$ T cells, gamma delta T cells, and activated dendritic cells. These findings corroborate the hyperactive adaptive immune response in pSD. This is consistent with some previous research results (55, 56). Zhang *et al*. have also found that the infiltration rate of activated dendritic cells in chronic inflammatory lesions of Sjogren's disease (SjD) is related to certain immune activity characteristics and high-risk factors for lymphoma (57).

The divergent correlations of hub genes with immune subsets, HADHA/JAK1/BRD4 with Tregs and ATG5/NRAS with $CD8^+$ T cells and DCs, suggest distinct functional axes. For instance, HADHA's negative correlation with gamma delta T cells implies mitochondrial dysfunction may dampen cytotoxic T-cell activity, while ATG5's association with activated DCs underscores its role in antigen presentation and B-cell activation. The AUC score based on hub genes further localised pyroptosis activity to monocytes, naive B cells, naive $CD8^+$ T cells, and naive $CD4^+$ T cells, emphasising their contribution to glandular inflammation and systemic autoimmunity. The pyroptosis process can connect innate immunity and adaptive immunity. The maturation and release of IL-1β can signal macrophages, activate and recruit them, and thereby affect the functions of immune cells, such as T cells, and the process of immune responses. It was suggested that the abnormal accumulation of DNA in pSD patients activates the inflammasome of haematopoietic monocytes and triggers pyroptosis as well as the secretion of pro-inflammatory cytokines IL-1β and IL-18 (58). In pSD, γδ T cells were significantly positively correlated with CASP3, indicating that pyroptosis may be involved in disease development by affecting specific immune cells (30). These immune correlates highlight potential biomarkers for monitoring disease activity and suggest immunomodulatory targets.

The integration of machine learning (LASSO, ElasticNet, RF, SVM) with SHAP interpretation provided a robust framework for biomarker discovery. Notably, the nomogram incorporating these genes demonstrated excellent calibration and clinical utility, offering a practical tool for risk stratification. Molecular docking identified CHX, danazol, and MP as potential drugs, with binding energies suggesting strong inhibitory potential. CHX is a widely used antibacterial agent, mainly used for oral care and skin disinfection. Since oral infections are common in patients with pSD, they can be controlled by using antibacterial drugs, such as CHX (59). In THP-1 monocytes stimulated by lipopolysaccharide, CHX significantly reduced the release of pro-inflammatory cytokines TNF, IL-1β, and IL-6, indicating that CHX has the potential to inhibit inflammatory responses (60, 61). Beyond its antimicrobial role, CHX's anti-pyroptotic potential via cytokine suppression warrants exploration in preclinical pSD models, particularly for managing oral manifestations and local inflammation. Danazol is a synthetic androgen, a derivative of the synthetic steroid ethisterone, that is often used in the treatment of endometriosis, fibrocystic breast disease, and hereditary angioedema. In autoimmune disease, such as pSD, it is often used to treat concurrent thrombocytopenia, and it has certain therapeutic effects in MRL/MpJ mice (62, 63). MP, as a synthetic glucocorticoid, has powerful anti-inflammatory and immunosuppressive effects. It is usually used in the acute and critical phases of pSD (64, 65). A study has found that MP can reduce the levels of IgG, erythrocyte sedimentation rate, and rheumatoid factor, and increase the salivary flow rate, thereby improving the EULAR Sjogren's Syndrome Patient Reported Index reported by patients with pSD (66). The molecular docking results provide a potential mechanism supporting its efficacy. However, the specific mechanism of action and application of these drugs in pSD still need to be further clarified through well-designed preclinical and clinical studies.

While our findings are promising, several limitations warrant consideration. Although we used multiple datasets for validation, the inherent heterogeneity of public GEO data may impact the specificity of results. Additionally, while single-cell RNA sequencing data helped analyse the expression characteristics of key genes, the relatively small sample size may restrict a comprehensive understanding of cell type-specific expression patterns. Moreover, the molecular docking studies, although providing initial clues for potential drugs, require further validation through in vitro and in vivo experiments to confirm their efficacy and safety. It is also important to note that our core discovery cohort was restricted to pSD, which sharpens the focus of our findings but necessitates caution when generalising to associated SjD.

Future research can be expanded in several directions. First, increasing the sample size and using more homogeneous datasets, particularly with more pSD-specific data, will enhance the reliability and specificity of the findings. Second, integrating multi-omics data, such as proteomics and metabolomics, can provide a more comprehensive understanding of the molecular mechanisms underlying pSD. Lastly, in-depth experimental studies, including cell function experiments and animal model validations, are needed to elucidate the mechanisms of action of key genes and potential drugs. Overall, we anticipate that these efforts will further advance the understanding of pSD pathophysiology and accelerate the clinical translation of novel diagnostic markers and therapeutic targets.

Conclusion

Our study underscores the involvement of pyroptosis-associated regulators in pSD development, identifying HADHA, JAK1, BRD4, ATG5, and NRAS as potential biomarkers. Their diagnostic value and interaction with immune cells were determined, and molecular docking confirmed their potential as therapeutic targets. These findings offer novel insights into the pathogenesis of pSD and lay the groundwork for future investigations and therapeutic development.

Acknowledgements

The authors would like to express their deepest appreciation to the GEO, GeneCards, AmiGO2, MSigDB, Genclip3, CIBERSORTx, Cellmarker2.0, GeneMANIA, NetworkAnalyst, Enrichr, Uniprot and PubChem for their provision of open-access resources, as well as to the editors and reviewers for their invaluable contributions to this work.

References

1. HOU J, FENG Y, YANG Z *et al*.: Primary Sjögren's syndrome: new perspectives on salivary gland epithelial cells. *Eur J Med Res* 2024; 29(1): 371. https://doi.org/10.1186/s40001-024-01967-5
2. RAMOS-CASALS M, BAER AN, BRITO-ZERÓN MDP *et al*.: 2023 International Rome consensus for the nomenclature of Sjögren disease. *Nat Rev Rheumatol* 2025; 21(7): 426-37. https://doi.org/10.1038/s41584-025-01268-z
3. MARIETTE X, CRISWELL LA: Primary Sjögren's syndrome. *N Engl J Med* 2018; 379(1): 97. https://doi.org/10.1056/nejmc1804598
4. GOULES AV, CHATZIS L, PEZOULAS VC *et al*.: Identification and evolution of predictors of Sjögren's disease-associated mucosa-associated lymphoid tissue lymphoma development over time: a case-control study. *Lancet Rheumatol* 2024; 6(10): e693-e702. https://doi.org/10.1016/s2665-9913(24)00183-8
5. BALDINI C, FULVIO G, LA ROCCA G, FERRO F: Update on the pathophysiology and treatment of primary Sjögren syndrome. *Nat Rev Rheumatol* 2024; 20(8): 473-91. https://doi.org/10.1038/s41584-024-01135-3
6. SONG Y, PENG Y, WANG B *et al*.: The roles of pyroptosis in the pathogenesis of autoimmune diseases. *Life Sci* 2024; 359(123232). https://doi.org/10.1016/j.lfs.2024.123232
7. YU S, WANG H, LIU M *et al*.: Loss of ATG5 in KRT14(+) cells leads to accumulated functional impairments of salivary glands via pyroptosis. *Faseb J* 2022; 36(12): e22631. https://doi.org/10.1096/fj.202200946R
8. HONG SM, LEE J, JANG SG *et al*.: Type I interferon increases inflammasomes associated pyroptosis in the salivary glands of patients with primary Sjögren's syndrome. *Immune Netw* 2020; 20(5): e39. https://doi.org/10.4110/in.2020.20.e39.
9. VAKRAKOU AG, SVOLAKI IP, EVANGELOU K, GORGOULIS VG, MANOUSSAKIS MN: Cell-autonomous epithelial activation of AIM2 (absent in melanoma-2) inflammasome by cytoplasmic DNA accumulations in primary Sjögren's syndrome. *J Autoimmun* 2020; 108(102381). https://doi.org/10.1016/j.jaut.2019.102381
10. LANGFELDER P, HORVATH S: WGCNA: an R package for weighted correlation network analysis. *BMC Bioinformatics* 2008; 9(559). https://doi.org/10.1186/1471-2105-9-559
11. YU G, WANG LG, HAN Y, HE QY: clusterProfiler: an R package for comparing biological themes among gene clusters. *Omics* 2012; 16(5): 284-87. https://doi.org/10.1089/omi.2011.0118
12. THE GENE ONTOLOGY RESOURCE: 20 years and still GOing strong. *Nucleic Acids Res* 2019; 47(D1): D330-38. https://doi.org/10.1093/nar/gky1055
13. KANEHISA M, GOTO S: KEGG: kyoto encyclopedia of genes and genomes. *Nucleic Acids Res* 2000; 28(1): 27-30. https://doi.org/10.1093/nar/28.1.27
14. FRIEDMAN J, HASTIE T, TIBSHIRANI R: Regularization paths for generalized linear models via coordinate descent. *J Stat Softw* 2010; 33(1): 1-22. https://doi.org/10.18637/jss.v033.i01
15. SVETNIK V, LIAW A, TONG C, CULBERSON JC, SHERIDAN RP, FEUSTON BP: Random-forest: a classification and regression tool for compound classification and QSAR modeling. *J Chem Inf Comput Sci* 2003; 43(6): 1947-58. https://doi.org/10.1021/ci034160g
16. SUYKENS JAK, VANDEWALLE J: Least squares support vector machine classifiers. *Neural Processing Letters* 1999; 9(3): 293-300. https://doi.org/10.1023/A: 1018628609742
17. NEWMAN AM, LIU CL, GREEN MR *et al*.: Robust enumeration of cell subsets from tissue expression profiles. *Nat Methods* 2015; 12(5): 453-57. https://doi.org/10.1038/nmeth.3337
18. STUART T, BUTLER A, HOFFMAN P *et al*.: Comprehensive Integration of Single-Cell Data. *Cell* 2019; 177(7): 1888-1902.e1821. https://doi.org/10.1016/j.cell.2019.05.031
19. HU C, LI T, XU Y *et al*.: CellMarker 2.0: an updated database of manually curated cell markers in human/mouse and web tools based on scRNA-seq data. *Nucleic Acids Res* 2023; 51(D1): D870-76. https://doi.org/10.1093/nar/gkac947
20. FRANZ M, RODRIGUEZ H, LOPES C *et al*.: GeneMANIA update 2018. *Nucleic Acids Res* 2018; 46(W1): W60-64. https://doi.org/10.1093/nar/gky311
21. KEENAN AB, TORRE D, LACHMANN A *et al*.: ChEA3: transcription factor enrichment analysis by orthogonal omics integration. *Nucleic Acids Res* 2019; 47(W1): W212-w224. https://doi.org/10.1093/nar/gkz446
22. LIU ZP, WU C, MIAO H, WU H: RegNetwork: an integrated database of transcriptional and post-transcriptional regulatory networks in human and mouse. *Database* (Oxford) 2015; 2015. https://doi.org/10.1093/database/bav095
23. XIE Z, BAILEY A, KULESHOV MV *et al*.: Gene set knowledge discovery with enrichr. *Curr Protoc* 2021; 1(3): e90. https://doi.org/10.1002/cpz1.90
24. YOO M, SHIN J, KIM J *et al*.: DSigDB: drug signatures database for gene set analysis. *Bioinformatics* 2015; 31(18): 3069-71. https://doi.org/10.1093/bioinformatics/btv313
25. TROTT O, OLSON AJ: AutoDock Vina: improving the speed and accuracy of docking with a new scoring function, efficient optimization, and multithreading. *J Comput Chem* 2010; 31(2): 455-61. https://doi.org/10.1002/jcc.21334
26. SEELIGER D, DE GROOT BL: Ligand docking and binding site analysis with PyMOL and Autodock/Vina. *J Comput Aided Mol Des* 2010; 24(5): 417-22. https://doi.org/10.1007/s10822-010-9352-6
27. BROZ P: Pyroptosis: molecular mechanisms and roles in disease. *Cell Res* 2025; 35(5): 334-44. https://doi.org/10.1038/s41422-025-01107-6
28. BAI Y, PAN Y, LIU X: Mechanistic insights into gasdermin-mediated pyroptosis. *Nat Rev Mol Cell Biol* 2025; 26(7): 501-21. https://doi.org/10.1038/s41580-025-00837-0
29. HU X, ZHANG H, ZHANG Q, YAO X, NI W, ZHOU K: Emerging role of STING signalling in CNS injury: inflammation, autophagy, necroptosis, ferroptosis and pyroptosis. *J Neuroinflammation* 2022; 19(1): 242. https://doi.org/10.1186/s12974-022-02602-y
30. CHEN W, CHEN W, XIA N, YAN R: Investigation of pyroptosis-related hub genes and the immune microenvironment in primary Sjögren's syndrome. *Clin Exp Rheumatol* 2024; 42(12): 2393-403. https://doi.org/10.55563/clinexprheumatol/3yu7pd
31. LIU Y, LU LL, WEN D *et al*.: Correction to: MiR-612 regulates invadopodia of hepatocellular carcinoma by HADHA-mediated lipid reprogramming. *J Hematol Oncol* 2020; 13(1): 44. https://doi.org/10.1186/s13045-020-00875-5
32. ZHANG Y, LV Y, ZHANG Q *et al*.: ALDH2 attenuates myocardial pyroptosis through breaking down Mitochondrion-NLRP3 inflammasome pathway in septic shock. *Front Pharmacol* 2023; 14(1125866). https://doi.org/10.3389/fphar.2023.1125866
33. MIAO EA, RAJAN JV, ADEREM A: Caspase-1-induced pyroptotic cell death. *Immunol Rev* 2011; 243(1): 206-14. https://doi.org/10.1111/j.1600-065X.2011.01044.x
34. HEID ME, KEYEL PA, KAMGA C, SHIVA S, WATKINS SC, SALTER RD: Mitochondrial reactive oxygen species induces NLRP3-dependent lysosomal damage and inflammasome activation. *J Immunol* 2013; 191(10): 5230-38. https://doi.org/10.4049/jimmunol.1301490
35. JOHNSON DC, OKONDO MC, ORTH EL *et al*.: DPP8/9 inhibitors activate the CARD8 inflammasome in resting lymphocytes. *Cell Death Dis* 2020; 11(8): 628. https://doi.org/10.1038/s41419-020-02865-4
36. MILLS KHG: IL-17 and IL-17-producing cells in protection versus pathology. *Nat Rev Immunol* 2023; 23(1): 38-54. https://doi.org/10.1038/s41577-022-00746-9
37. HONG Y: The role of mitochondria-related proteins in inflammation and autoimmune diseases: a causal analysis using Mendelian randomization and colocalization. *Health Inf Sci Syst* 2025; 13(1): 42. https://doi.org/10.1007/s13755-025-00358-2
38. XU H, ZHANG X, WANG X *et al*.: Cellular spermine targets JAK signaling to restrain cytokine-mediated autoimmunity. *Immunity* 2024; 57(8): 1796-811.e1798. https://doi.org/10.1016/j.immuni.2024.05.025
39. LEE J, LEE J, KWOK SK *et al*.: JAK-1 Inhibition suppresses interferon-induced BAFF production in human salivary gland: potential therapeutic strategy for primary Sjögren's syndrome. *Arthritis Rheumatol* 2018; 70(12): 2057-66. https://doi.org/10.1002/art.40589
40. DIENZ O, EATON SM, BOND JP *et al*.: The induction of antibody production by IL-6 is indirectly mediated by IL-21 produced by $CD4^+$ T cells. *J Exp Med* 2009; 206(1): 69-

78. https://doi.org/10.1084/jem.20081571
41. HOWARD TRIPP N, TARN J, NATASARI A, GILLESPIE C *et al*.: Fatigue in primary Sjögren's syndrome is associated with lower levels of proinflammatory cytokines. *RMD Open* 2016; 2(2): e000282. https://doi.org/10.1136/rmdopen-2016-000282
42. BERGSBAKEN T, FINK SL, COOKSON BT: Pyroptosis: host cell death and inflammation. *Nat Rev Microbiol* 2009; 7(2): 99-109. https://doi.org/10.1038/nrmicro2070
43. BARRAT FJ, CROW MK, IVASHKIV LB: Interferon target-gene expression and epigenomic signatures in health and disease. *Nat Immunol* 2019; 20(12): 1574-83. https://doi.org/10.1038/s41590-019-0466-2
44. LI WX: Canonical and non-canonical JAK-STAT signaling. *Trends Cell Biol* 2008; 18(11): 545-51. https://doi.org/10.1016/j.tcb.2008.08.008
45. CLARK JD, FLANAGAN ME, TELLIEZ JB: Discovery and development of Janus kinase (JAK) inhibitors for inflammatory diseases. *J Med Chem* 2014; 57(12): 5023-38. https://doi.org/10.1021/jm401490p
46. MOK CC: The Jakinibs in systemic lupus erythematosus: progress and prospects. *Expert Opin Investig Drugs* 2019; 28(1): 85-92. https://doi.org/10.1080/13543784.2019.1551358
47. BALDINI C, MORICONI FR, GALIMBERTI S, LIBBY P, DE CATERINA R: The JAK-STAT pathway: an emerging target for cardiovascular disease in rheumatoid arthritis and myeloproliferative neoplasms. *Eur Heart J* 2021; 42(42): 4389-400. https://doi.org/10.1093/eurheartj/ehab447
48. GUPTA S, YAMADA E, NAKAMURA H *et al*.: Inhibition of JAK-STAT pathway corrects salivary gland inflammation and interferon driven immune activation in Sjögren's disease. *Ann Rheum Dis* 2024; 83(8): 1034-47. https://doi.org/10.1136/ard-2023-224842
49. HAO K, JIANG W, ZHOU M *et al*.: Targeting BRD4 prevents acute gouty arthritis by regulating pyroptosis. *Int J Biol Sci* 2020; 16(16): 3163-73. https://doi.org/10.7150/ijbs.46153
50. DAI C, SUN J, YANG G *et al*.: The total xanthones from Gentianella acuta alleviate acute myocardial infarction by targeting BRD4-mediated cardiomyocyte pyroptosis and inflammation. *Phytomedicine* 2025; 147(157156). https://doi.org/10.1016/j.phymed.2025.157156
51. WANG J, ZHANG L, LIU Y *et al*.: Epithelial Atg5 deficiency intensifies caspase-11 activation, fueling extracellular mtDNA release to activate cGAS-STING-NLRP3 axis in macrophages during pseudomonas infection. *MedComm* (2020). 2025; 6(7): e70239. https://doi.org/10.1002/mco2.70239
52. TANG Q, LIU W, YANG X *et al*.: ATG5-mediated autophagy may inhibit pyroptosis to ameliorate oleic acid-induced hepatocyte steatosis. *DNA Cell Biol* 2022; 41(12): 1038-52. https://doi.org/10.1089/dna.2022.0265.
53. YANG J, WANG C, ZHANG Y, CHENG S, XU Y, WANG Y: A Novel pyroptosis-related signature for predicting prognosis and evaluating tumor immune microenvironment in ovarian cancer. *J Ovarian Res* 2023; 16(1): 196. https://doi.org/10.1186/s13048-023-01275-2
54. LI A, MA Y, JIN M *et al*.: Activated mutant NRas(Q61K) drives aberrant melanocyte signaling, survival, and invasiveness via a Rac1-dependent mechanism. *J Invest Dermatol* 2012; 132(11): 2610-21. https://doi.org/10.1038/jid.2012.186
55. CHENG C, ZHOU J, CHEN R *et al*.: Predicted disease-specific immune infiltration patterns decode the potential mechanisms of long non-coding RNAs in primary Sjögren's syndrome. *Front Immunol* 2021; 12(624614. https://doi.org/10.3389/fimmu.2021.624614
56. HONG X, MENG S, TANG D *et al*.: Single-cell RNA sequencing reveals the expansion of cytotoxic CD4(+) T lymphocytes and a landscape of immune cells in primary Sjögren's syndrome. *Front Immunol* 2020; 11(594658). https://doi.org/10.3389/fimmu.2020.594658
57. ZHANG N, JI C, BAO X, PENG X, TANG M, YUAN C: Uncovering potential new biomarkers and immune infiltration characteristics in primary Sjögren's syndrome by integrated bioinformatics analysis. *Medicine* (Baltimore) 2023; 102(41): e35534. https://doi.org/10.1097/md.0000000000035534
58. HONG Y, CHEN S, JIANG X *et al*.: Exosomes as immunomodulators in autoimmune inflammation: implications for primary Sjögren's disease. *Inflamm Res* 2025; 74(1): 91. https://doi.org/10.1007/s00011-025-02053-0
59. PRICE EJ, RAUZ S, TAPPUNI AR *et al*.: The British Society for Rheumatology guideline for the management of adults with primary Sjögren's syndrome. *Rheumatology* (Oxford) 2017; 56(10): 1643-7. https://doi.org/10.1093/rheumatology/kex163
60. RAPS S, BAHR L, KARKOSSA I, ROSSOL M, VON BERGEN M, SCHUBERT K: Triclosan and its alternatives, especially chlorhexidine, modulate macrophage immune response with distinct modes of action. *Sci Total Environ* 2024; 914(169650). https://doi.org/10.1016/j.scitotenv.2023.169650
61. SANTIAGO KB, CONTI BJ, CARDOSO EO, GOLIM MA, SFORCIN JM: Immunomodulatory/anti-inflammatory effects of a propolis-containing mouthwash on human monocytes. *Pathog Dis* 2016; 74(8). https://doi.org/10.1093/femspd/ftw081
62. ZANELLA A, BARCELLINI W: Treatment of autoimmune hemolytic anemias. *Haematologica* 2014; 99(10): 1547-54. https://doi.org/10.3324/haematol.2014.114561
63. CONNOLLY KM, STECHER VJ, SNYDER BW, BOHNET E, POTTS GO: The effect of danazol in the MRL/lpr mouse model of autoimmune disease. *Agents Actions* 1988; 25(1-2): 164-70. https://doi.org/10.1007/bf01969108
64. DOOLAN G, FAIZAL NM, FOLEY C *et al*.: Treatment strategies for Sjögren's syndrome with childhood onset: a systematic review of the literature. *Rheumatology* (Oxford) 2022; 61(3): 892-912. https://doi.org/10.1093/rheumatology/keab579
65. ZHU GQ, HU RX, PENG Y, YAO Y, LI GM: A Chinese girl with neuromyelitis optica spectrum disorder coexisting with primary Sjögren's syndrome: a case report and literature review. *Front Immunol* 2025; 16(1559825. https://doi.org/10.3389/fimmu.2025.1559825
66. LI CJ, LI R, LIU HZ, CHENG CF, ZHAO T: Clinical effect of methylprednisolone combined with Iguratimod in the treatment of Primary Sjögren's syndrome and its effect on the levels of serum immunoglobulin. *China Pharmaceuticals* 2018; 027(014): 35-37.